

Flow Induced Material Degradation In Power Plant Secondary Systems-A Review

I. S. Kim

Korea Advanced Institute of Science and Technology
373-1 Kusong-dong, Yusong-gu, Taejon 305-701, Korea

M. Van Der Helm and R. G. Ballinger

Massachusetts Institute of Technology
77 Massachusetts Avenue, Cambridge, MA02139, U.S.A.

(Received November 25, 1997)

Abstract

Flow Induced Material Degradation (FIMD) is reviewed focusing on Flow Accelerated Corrosion (FAC) models. Several examples of FAC related incidents are described, which include nuclear and fossil power plants. Lastly, mitigation techniques such as inspection, material selection, water chemistry, temperature, and hydrodynamic factor are discussed.

1. Introduction

Flow Induced Material Degradation (FIMD), as it applied to degradation of low alloy steel piping in steam power plants, is a term which encompasses several phenomena, all of which, result in degradation of the piping through material loss. These phenomena include cavitation, flow accelerated corrosion (FAC), abrasion corrosion, and droplet impingement. This class of phenomena has resulted in premature piping failures, extended outages for maintenance, and in a few cases catastrophic failures that have resulted in injury and fatalities [1]. While FIMD is a generic problem in all steam power plants, it is especially troublesome in nuclear power plants due to the cost of maintenance. As a result a considerable effort has been made by the industry to understand, model, and make alterations in plant chemistry to mitigate the problem. In this paper

we present a general review of the FIMD phenomena with an emphasis on flow assisted corrosion (FAC) since, of the four processes mentioned above, FAC is most insidious. Following the general review we present several examples of FAC related failures in the nuclear power plants as well as in fossil plants. Lastly, mitigation methods are discussed.

2. Flow Induced Material Degradation

As mentioned above, four Flow Induced Material Degradation (FIMD) phenomena have been identified. These phenomena are FAC, cavitation, droplet impingement, and abrasion corrosion. Three phenomena, cavitation, FAC, and droplet impingement are more prevalent in secondary steam piping. Cavitation, abrasion corrosion, and FAC are single phase phenomena; and abrasion corrosion, FAC, and droplet impingement are two

phase phenomena.

Cavitation

Cavitation, solely a single phase flow phenomena, involves the repeated formation and collapse of vapor bubbles and this collapse causes the generation of shock waves that cause material deformation and removal. Sharp, jagged surfaces characterize the wear damage. The expected location for this phenomena is downstream of control valves, orifices, pumps, expanders, and elbows, where local increases in velocity causes static pressure reduction. Static pressure restoration downstream of the component causes vapor collapse. A cavitation factor can be defined as:

$$C = \frac{\Delta P}{p_0 - p_v(T_0)} \quad (1)$$

where

Δp = pressure drop across the component

p_0 = static pressure within component

$p_v(T_0)$ = the saturated pressure at the fluid temperature within the component

A cavitation factor of less than 1/5 indicates the likelihood of cavitation. Proper prediction of cavitation requires specific knowledge and modeling of the component as this phenomenon is a strong function of the component's geometry. Figure 1 shows the variety of bubble formation and collapse locations within the component or pipe [2]. A local decrease in pressure results in the formation of bubbles. A subsequent pressure increase can result in the unstable collapse of the bubbles and the generation of high (locally) velocity fluid jets that can physically remove material.

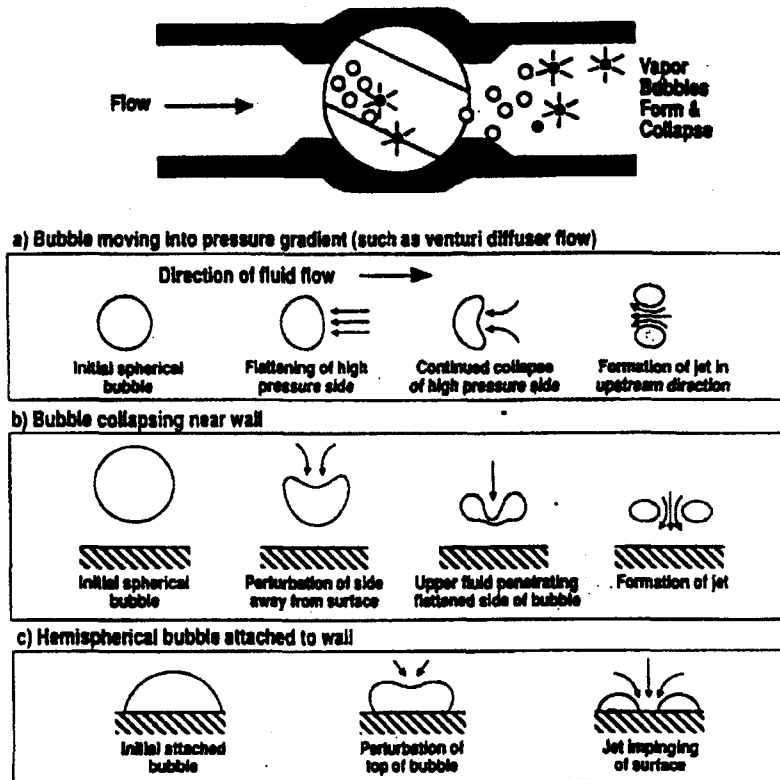


Fig. 1. Forms of Cavitation Material Degradation [4].

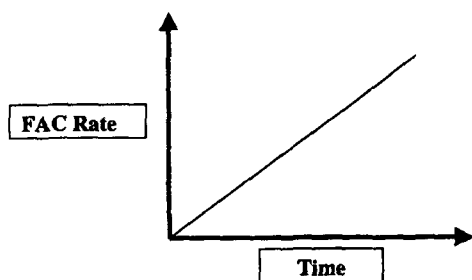


Fig. 2. History Characteristics of Flow Accelerated Corrosion

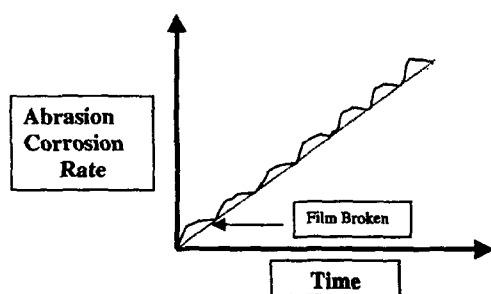


Fig. 3. History Characteristics of Abrasion Corrosion

Flow Accelerated Corrosion

Flow accelerated corrosion (FAC) in carbon steel piping systems is characterized by the simultaneous dissolution of iron from the iron oxide-fluid interface and the formation of an iron oxide film at the oxide-metal interface. Bulk flow plays a vital role in providing a sink (gradient in concentration) for the dissolution products or insuring removal of these products. Under stagnant conditions, corrosion products would concentrate in the aqueous solution reducing the concentration gradient driving force for the corrosion process. Flow inhibits this concentration process and enhances the concentration gradient. Figure 2 shows a schematic of a typical steady state material loss as

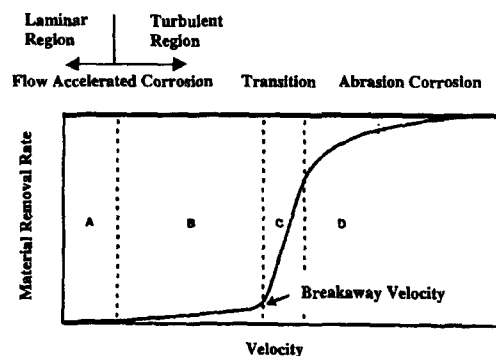


Fig. 4. Material Removal Rate as a Function of Velocity for FAC and Abrasion Corrosion [3]

a function of time assumed to exist for the FAC process under constant chemistry and thermal hydraulic conditions [3].

Wear patches often start as horseshoe or scallop shapes expanding to wide troughs of dimension less than the order of the pipe diameter [2]. Two phase material degradation appears as 'tiger striping' occurring in bends and downstream from flow disruptions. The degradation often takes the form of separate patches on the order of the pipe diameter. These regions often experience significantly greater material loss than immediately adjacent sections. Tiger striping is a phenomenon which has yet to be adequately explained.

An additional acceleration may occur when rapid flashing of water to vapor occurs. This phenomenon is aggravated by system pressure fluctuations. Increased fluid velocity, approaching sonic velocity, accelerates FAC [4]. Models of FAC will be discussed in more detail below.

Abrasion Corrosion

Abrasion corrosion involves the mechanical removal of the protective oxide film by particles within the flow as a result of impingement on the oxide. Removal of the oxide followed by oxide

reformation results in a continuous removal of material. Figure 3 illustrates the typical time history of thickness reduction with a greater slope indicating oxide removal by impingement and a lesser slope indicating oxide reformation. The resulting process is quasi steady state.

Figure 4 illustrates the respective velocity regimes where FAC and abrasion corrosion are dominant. Abrasion corrosion occurs at high velocities and results in significant increase in material loss when compared to FAC loss rates occurring at lower velocities. Note the presence of a critical velocity above which abrasion corrosion occurs. Contributing factors include particle size and structure, material toughness, and inclination of flow relative to the surface. Copper and brass alloys are more likely affected by this mechanism [3].

Droplet Impingement

Droplet Impingement is a degradation type for which two phase flow must exist. Entrained droplets from the liquid phase are propelled due to the vapor phase at velocities significant enough to cause material fatigue. Keck measured a variety of droplet wear rates for a range of velocities and angles for two different geometries [5]. Modifying a model suggested by Sanchez-Caldera [6], incorporating data taken, and using Keller's geometric factors from the literature [7], two phase droplet velocity, entrainment fraction, and magnetite properties, Keck determined the wear coefficient using the following relation for material loss per unit area:

$$\dot{m}'' = \frac{C \cdot \rho_f \cdot \dot{m}_{tot} \cdot (1-x) \cdot V_d^4 \cdot F_e \cdot F_h \cdot \rho_{ox}}{(P \cdot \epsilon_c)^2 \cdot A_c} \quad (2)$$

where:

- \dot{m}'' = wear rate per unit area [kg/m²/sec],
- C = wear coefficient derived empirically,

- ρ_f = fluid density [kg/m³],
- \dot{m}_{tot} = total mass flow rate [kg/sec],
- x = flow quality,
- V_d = droplet velocity [m/sec],
- F_e = entrained fraction,
- F_h = fraction impacting surface,
- ρ_{ox} = oxide density [kg/m³],
- P = indentation hardness [N/m²],
- ϵ_c = critical strain to fracture,
- A_c = characteristic wear area [m²].

Droplet impingement exhibits two primary characteristics. The first is that material removal rates may be quite rapid. Second, damage due to droplet impingement is most often observed as 'sharp and jagged damage to a surface which is mostly metallically smooth' [8].

3. FAC Models

A variety of models have been proposed to describe FAC, both empirical and mechanistic. Empirical models are based on a statistical fit to laboratory data trends which are then modified as appropriate to match plant data. Mechanistic models establish a set of interrelated equations describing the physical processes occurring at particular locations within a proposed system. While empirical models may fit data well, extrapolation of trends to the full function space may not be accurate. For example, the effect of velocity at low and high pH may be very different because of changes in film stability. While mechanistic models allow the investigator to incorporate all relevant mechanisms, they may produce a set of equations too cumbersome to solve in a reasonable amount of time. In the beginning of model development, mechanistic models provide insight into the phenomena and direction to experimentation. Statistical approaches based on the data, however, provide a more useable end product for industry.

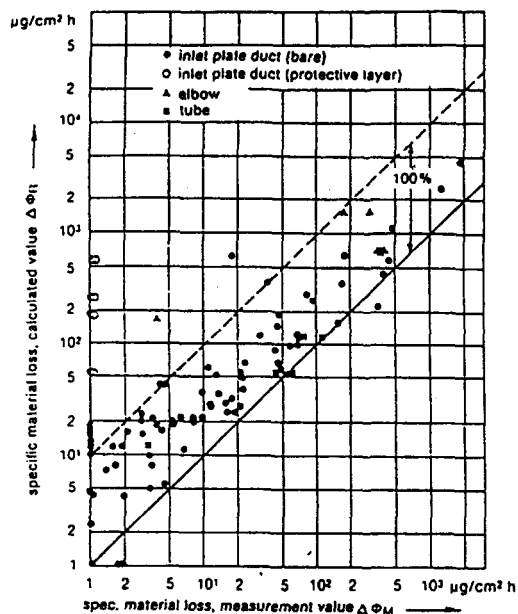


Fig. 5. Comparison of Predicted and Measured Material Degradation by the Kastner Model for Single Phase Lab Data [9]

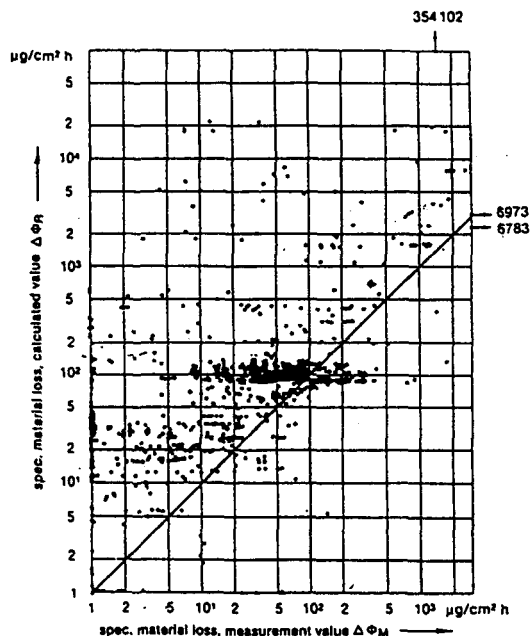


Fig. 6. Comparison of Predicted and Measured Material Degradation by the Kastner Model for Single and Two Phase Lab and Plant Data [9]

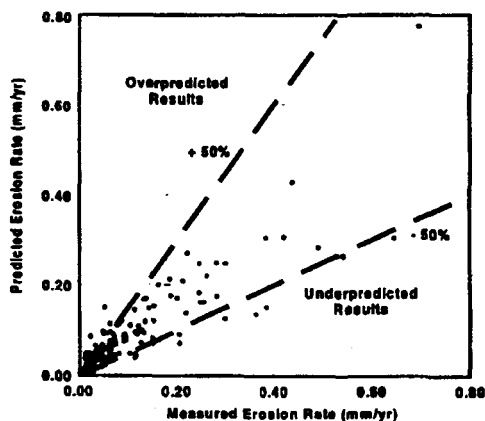


Fig. 7. Comparison of Predicted and Measured Material Degradation by the Chexal-Horowitz Model for Single Phase Lab Data [3]

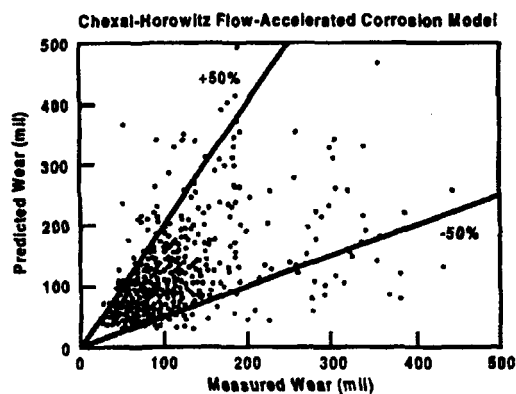


Fig. 8. Comparison of Predicted and Measured Material Degradation by the Chexal-Horowitz Model for Single and Two Phase Lab and Plant Data [3]

Empirical Models

Of the many models proposed to describe

FAC, four will be briefly discussed in this section. The four models are those from Kastner [9], Chexal-Horowitz, (CH) [3], Sanchez-

Caldera, (SC) [6], and Bignold [10]. The Kastner and Chexal-Horowitz models are empirical while the Sanchez-Caldera and Bignold models are mechanistic. Table 1 shows the variables that are included in each of these models. The Kastner model is the FAC model that serves as the basis of the WALTHERC code produced by Siemens/KWU as a program to aid utilities in managing pipe degradation caused by FAC. The Kastner model is derived from both single and two phase flow data. Single phase flow data taken in the lab was used to derive the original relationship. The derived relationships were then adjusted as needed to fit two phase plant data [9]. The laboratory data used in the Kastner model was generated at Siemens/KWU and the plant data used consists of approximately 6000 single and two phase data points [3]. The final Kastner model is a separable equation of the form:

$$\dot{m}'' = F_1(v, T, allcont) \cdot F_2(pH) \cdot F_3(O_2) \cdot F_4(G) \cdot F_5(x) \quad (3)$$

which is a function of velocity (v), temperature (T), alloy content, pH, oxygen content (O_2), geometry (G), and water quality (x), respectively.

A similar method was used in the derivation of the CH model which is the FAC model within the CHECWORKS code, developed by the Electric Power Research Institute (EPRI). The data used by EPRI includes 'pertinent' British, French and German lab data, U. S. plant data, and EPRI sponsored lab data [3]. The final form of the CH model is a separable equation of the form:

$$\dot{m}'' = F_1(T) \cdot F_2(pH) \cdot F_3(allcont) \cdot F_4(k) \cdot F_5(O_2) \cdot F_6(G) \cdot F_7(\alpha) \quad (4)$$

where k is the mass conductance and α is the void fraction of the flow.

Both the Kastner and CH model report better model predictions when compared to laboratory single phase data than when compared to all data within their respective databases. Figures 5 and 6 show a comparison, respectively, of single phase lab data and both lab and plant data to the Kastner model. Figures 7 and 8 show a comparison, respectively, of single phase lab data and both lab and plant data to the CH model. Data shown in figures 5 and 7 are a subset of that in figures 6 and 8, respectively. The outlying data, data for which the models predicts little wear yet actually experience significant wear, is of particular concern. As indicated from figures 6 and 8, these outliers are likely two phase data for which the physical degradation mechanisms (e.g. the cause of tiger striping) is not well understood.

Mechanistic Models

Sanchez-Caldera Model

Sanchez-Caldera models the FAC process as a coupled kinetically limited mass transfer process. The transfer rate of material from the pipe to the bulk fluid flow is modeled as a one dimensional steady state process. The process is assumed to take place in two steps: (1) kinetically limited dissolution of iron to produce ferrous ion followed by (2) mass transfer of the ferrous ion to the bulk flow by ion migration and convection. Figure 9 shows a schematic of the model. The process can be modeled as a series of mass transfer processes through resistances to the transfer process as depicted in the "circuit" diagram at the base of Figure 9.

The metal dissolution to the metal-oxide interface is assumed to be first order with respect to concentration such that ferrous ion production at the metal-oxide interface is proportional to the difference between two concentrations, C_{eq} and

Table 1. Comparison of Models Based on Primary Variables Modeled. Note that (a) Indicates a Value Included Numerically but not Varied Experimentally, (b) Indicates that Cr and Mo were Considered Together and, (c) Indicates that Cr, Mo, and Cu were Considered Separately

	Kastner	Chexal-Horowitz	Sanchez-Caldera	Bignold
pH	X	X	X ^a	X
Oxygen	X	X		
Velocity	X	X	X	X
Temperature	X	X	X	X
Alloy Chemistry	X ^b	X ^c		
Geometry	X	X	X ^a	X
Pipe Diameter		X	X ^a	X
Time	X			

C_{mo} . The relationship for material removal rate is then:

$$\dot{m}'' = K^* (C_{eq} - C_{mo}) \quad (5)$$

The proportionality constant, denoted K, is the reaction rate which is assumed to follow an Arrhenius Law:

$$K = Ae^{-\frac{E}{R \cdot T}} \quad (6)$$

The constants A and E were determined by fitting the SC model to data. C_{eq} shown in Figure 9 corresponds to the equilibrium concentration of ferrous ion at the metal-oxide interface as

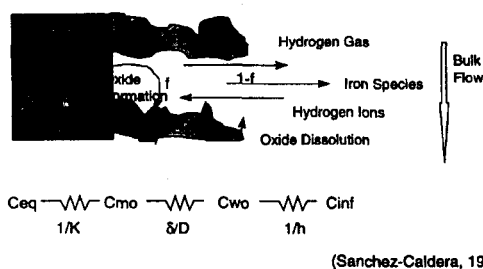
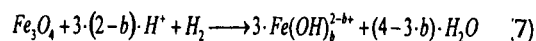


Fig. 9. Schematic of the FAC Process as described by the Sanchez-Caldera Model

described by the ferrous hydroxide formation reaction set [11]:



for $b = 0, 1, 2, 3$, given the concentration of hydrogen ions and hydrogen gas at the interface. C_{mo} corresponds to the ferrous ion concentration that exists at the metal-oxide interface given the concentration of hydrogen ions and hydrogen gas at the interface.

The mass transfer resistance controlled step consists of diffusion through an oxide layer to the oxide-fluid interface and convection to the bulk fluid. A competing pathway for ferrous ion removal at the metal-oxide interface is the production of magnetite according to the reverse of the Equation 7. This process creates the oxide layer. A fraction, f , of the ferrous ions at the metal-oxide interface are used in the formation of magnetite. The remaining fraction of ferrous ions, $1-f$, are removed by the mass transfer step described above. Figure 8 shows the diffusion resistance through the oxide, (δ/D) , for transport from the metal-oxide interface to the water-oxide interface due to the concentration difference,

$C_{mo} - C_{wo}$, at the two interfaces. In this resistance relation, δ is the oxide thickness and D is the diffusion coefficient for ferrous ions through the oxide. The convection resistance, $1/h$, corresponds to the mass transfer from the water-oxide interface to the bulk fluid, due to concentration difference, $C_{wo} - C_{inf}$, at the two interfaces. The bulk fluid motion enhances this mass transfer. The following relation describes the overall mass transfer:

$$\dot{m}'' = \frac{C_{eq} \cdot \theta(T)}{1/K + (1-f) \cdot \left[\frac{\delta}{D} + \frac{1}{h} \right]} \quad (8)$$

where C_{eq} is assumed to be much greater than C_{inf} and \dot{m}'' is the material removal rate per unit area. The porosity of the oxide on the metal-oxide interface is denoted by $\theta(T)$ and is assumed to be a function of temperature. As the porosity decreases available area for mass transfer decreases so that the overall iron dissolution rate decreases.

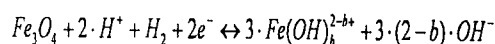
In a similar manner as described above, hydrogen ions are transferred to the metal-oxide interface from the bulk fluid and hydrogen gas is transferred from the metal-oxide interface to the bulk fluid. Assumptions are made about the bulk fluid hydrogen gas concentration and the hydrogen ion concentration is determined from measured pH. The diffusion coefficients used to model the mass transfer processes correspond to that of hydrogen ions and gas in water.

At low temperatures the production of ferrous ions at the metal-oxide interface is dissolution rate limited (i.e. a low value of K). At high temperatures, the oxide porosity decreases, limiting the dissolution of the metal. The peak in FAC occurs near 150 °C [6]. Sanchez-Caldera matches his model parameters to the values determined in his experiments to evaluate constants in the model.

Bignold Model

The Bignold model [10] is the only mechanistic model that considers the electrochemical aspects of the corrosion process. Noting the coupling of potential, ion concentration, and current of the oxidizing and reducing species, Bignold derives a relationship between the FAC rate and the mass transfer conductance. The mass transfer resistance (the inverse of the conductance) operates in series with a kinetic resistance as in the SC model. As in the SC model mass transfer resistance limits the process at high temperature and the kinetic resistance limits the process at low temperature.

Bignold model assumes a series process of (1) oxide formation at the metal-oxide surface, (2) oxide dissolution at the oxide-solution interface and (3) convection of ferrous ions and ferrous hydroxides to the bulk flow. In the last step, convection to the bulk flow is assumed to be rate limiting at high temperature. Bignold considers the following set of reactions for the dissolution of magnetite:



for $b = 0, 1$, and 2 . Bignold uses the Nernst equation to derive an expression that relates the half cell electrode potential, E , of the cathodic reactions to the total of ferrous hydroxide species from the various reactions:

$$C_S = C_{eq}'' \cdot [H^+]^{2/3} \cdot e^{\frac{-2 \cdot F \cdot E}{3 \cdot R \cdot T}} \quad (10)$$

where the total ferrous species, C_S , is given by:

$$C_S = \sum_{b=0}^2 Fe(OH)_b^{(2-b)+} \quad (11)$$

In Equation 10, F is Faraday's constant, R is the gas law constant, and T is absolute temperature.

Table 2. Piping and Components Susceptible to FAC [3]

Piping		Components	Other
1(Systems	2(Systems		
Condensate &Feed	HP & LP Extraction	MS Reheater	Cross-Under
Aux Feed	Flashing Lines to	FW Heater Drains	Downstream of
	Condenser		Flow Meters
Heater Drains	FW Heater Vents	Steam Generator	Downstream of
			Control Valves
MS Drains		Pumps	Bypass Lines
S/G Blowdown			
Reheater Drains			
Other Drains			

Equation 10 satisfies charge balance among the various ferrous hydroxides and ions produced by Equation 9.

The Bignold model then assumes that the current due to the cathodic discharge reaction of hydrogen ions producing hydrogen gas (which balances the total reaction of anodic dissolution of ferrous ions originating from the metal) is proportional to the exponential of the half cell electrode potential, E :

$$i_c = -F \cdot B(pH) \cdot e^{\frac{-F \cdot E}{R \cdot T}} \quad (12)$$

where $B(pH)$ is a function of pH determined from experimental data. Bignold then balances this current with the convection limited dissolution of magnetite to derive a FAC rate proportional to the cube of the mass transfer conductance. Bignold provides data to support this trend in FAC rate with mass transfer conductance.

Neither the Bignold nor the SC model includes the effect of oxygen content of the fluid or alloy content of the metal. Neither model properly describes velocity effects at low temperatures. At low temperatures, experimental data show the

FAC rate to be velocity dependent, which is not a characteristic of either mechanistic model.

Areas Susceptible to FAC

As summarized by Chexal, a number of piping systems and components of the secondary system have been historically affected by FAC [3]. Table 2 lists those systems. When determining the most susceptible areas in the plant, one should expect a number of the listed locations to be critical. It should be emphasized, however, that the critical areas for any given plant are not limited to those listed in Table 2.

4. Examples of Flow Accelerated Corrosion in Power Plants

According to SKI Report [12, 13] out of 1500 reported piping failures in U.S. nuclear power plants over the last 35 years 295 cases were caused by FAC, of which 95 occurred at BWRs and 200 occurred at PWRs. As is well known, the Surry 2 plant accident in 1986 compelled U.S. NRC to recommend that utilities adopt appropriate FAC monitoring programs. The

programs developed by either EPRI, EDF, and Siemens have been instituted at essentially all PWR units. A survey by Jonas [14], indicated that over 50% of plants have experienced FAC in feedwater piping and 97% have experienced FAC in wet steam piping. Simplified approaches to the prediction of FAC have proven unsatisfactory because there exist wide varieties of flow conditions, water chemistry, material compositions and, additionally, human errors. While nuclear power plants are rather well regulated and under strict service schedules which require component inspections on a regular basis, fossil power plants often utilize shorter, irregularly spaced maintenance outages [15]. In the following sections we discuss selected examples of FAC to place the problem in perspective before discussing remedial measures.

Heater Drain Pump Discharge Piping at the Trojan Station

A pipe rupture caused by FAC was reported at Trojan Station in a 14 inch (35.5 cm) diameter heater drain pump discharge pipe. The incident occurred on March 9, 1985. Following a turbine trip the automatic main feedwater produced a pressure pulse to approximately 875 psi (6 MPa) in the heater drain and feedwater systems. The pressure surge caused a degraded (thinned) section of the piping to rupture, which resulted in the release of a steam at 350(F (177 °C). One individual received burns on 50% of his body. The cause of the failure was identified as single phase FAC. The degradation occurred very close to a weld on the pipe, which was made of SA106 Gr B material. The alloying content of the failed pipe was very low in Cr, Mo, Ni, and Cu. The eroded inside surface of the pipe clearly showed a scalloped surface

typical of FAC.

Moisture Separator Drain Line at Millstone Unit 3

Millstone Unit 3 is 1154 MWe, 4 loop Westinghouse PWR that began commercial operation on April 23, 1986. On December 31, 1990 a multiple (2) pipe rupture occurred in the DSM system (Moisture Separator Reheater drain line) [16], which returns water collected by the turbine generator moisture separators to the condensate header. The flow in the 6 inch (15 cm) discharge pipes consisted of 380(F (193 °C) liquid at a normal velocity of 17 ft/sec (5.1 m/sec). These flow conditions made these pipes susceptible to thinning by FAC. These pipes were not identified as susceptible when analyzed using then currently available FAC models. The pipe breaks were preceded by a pencil-size leak that existed for approximately three hours. Inspection revealed that the piping had experienced severe FAC. In the area where the breaks occurred, piping thickness was eroded to approximately 0.020 inches (0.51 mm) from original design specification of 0.280 inches (7.1 mm).

Moisture Separator Reheater Drain Line at Millstone Unit 2

On November 6, 1991 a 8 inch (20.3 cm) reheater drain line rupture occurred in an elbow at Millstone 2 [17]. The failed line (B train) and parallel sister line (A train) had been in service since 1975, and no UT inspection had been performed on these lines since installation. A laboratory analysis found a difference in the trace chromium content between 0.01% (failed pipe) and 0.04% (unfailed pipe). In the failed B train a joint mismatch and weld backing ring resulted in a step of close to 3/8 inches (9.5

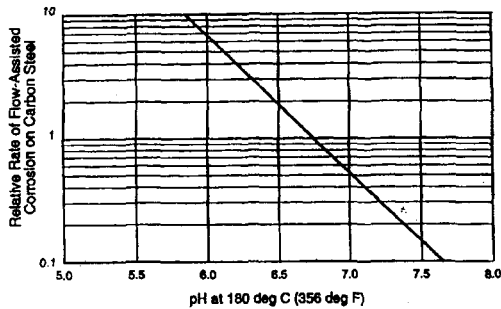


Fig. 10. Effect of pH on the Rate of FAC of Carbon Steel [17]

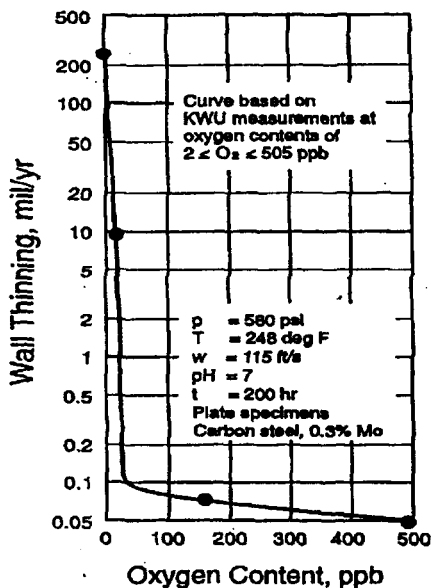


Fig. 12. Effect of Oxygen Content on the Rate of FAC in Carbon Steel [18]

mm). Local flow turbulence in a two phase fluid resulted in gas stripping or partitioning of gasses oxygen and ammonia from the liquid phase to the steam phase. On the other hand, in train A the joint mismatch was much smaller and without the weld backing ring. When the local pH (hot) was reduced from 6.5 to 6.0 by the

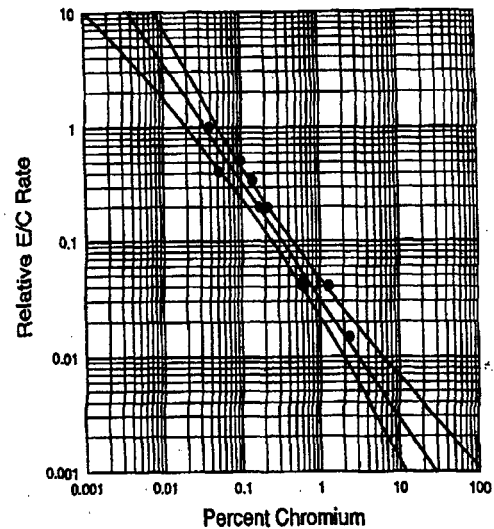


Fig. 11. Effect of Chromium Content on the FAC Rate of Carbon Steel [18]

ammonia partition, the relative rate of FAC was estimated to have increased by a factor of 3. This is illustrated in Figure 10 which shows the dependence of FAC on pH. The chromium content difference would also have resulted in an increase in the degradation rate by a factor of approximately 3.5 times as is illustrated in Figure 11. The difference in the wear observed between two different elbows, one that failed and one that did not, was a factor of 3.7 (0.283 inch (6.04 mm) wear on failed elbow and 0.075 inch (1.9 mm) on the unfailed elbow). Furthermore, extremely low oxygen concentrations (close to zero) caused by gas stripping as a result of turbulence would also have resulted in an accelerated wear rate in the failed elbow in B train. The effect of oxygen concentration on FAC is shown in Figure 12.

It was postulated that the flow turbulence in the two-phase fluid resulted in partitioning of gasses such as oxygen and ammonia from the liquid phase to steam leaving a fluid on the pipe

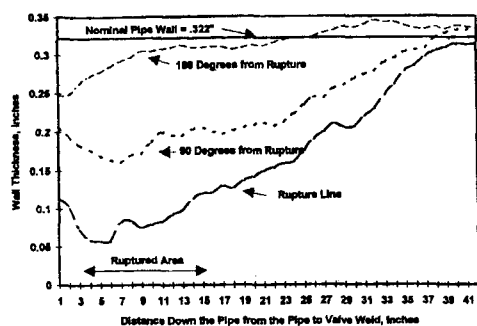


Fig. 13. Wall Thickness Variation Down the Pipe to Valve Weld [18]

surface which is more aggressive to FAC. Synergistically, the trace (0.01%) levels of chromium in the failed carbon steel elbow were believed to have accelerated the wear rate.

Heater Drain Line at Millstone Unit 2

A formal Flow-Accelerated Corrosion (FAC) program has been in place at Millstone Unit 2 since 1991. Yet, the unit experienced a pipe break in a heater drain pump recirculation line in August 1995 [18]. A water hammer increased the line pressure to the point that a section of pipe near a valve that had a significant wall thinning due to FAC ruptured. UT wall thickness measurement results, shown in Figure 13, shows the amount of wall thinning of the failed section of pipe in the rupture region and 90 degrees and 180 degrees from the rupture. The surface of the pipe wall close to the rupture showed a black, shining scalloped appearance which is typical of FAC. The fact that most of the wall thinning occurred in the region close to the valve (opposite from the side of the gate) indicates that the flow conditions in this region were more aggressive than in the rest of the pipe. During operation the gate valve would have been normally closed (no flow) or

fully open (fairly uniform flow with low turbulence). Based on the one sided nature of the FAC damage to the pipe wall it is apparent that the valve had been inadvertently left open for periods of time or may have been used to throttle flow. The pipe rupture was due to tensile overload and failure in the area of localized pipe thinning, which was caused by FAC. The thinning condition was maintained by operation with a partially open or leaking by gate valve. The pressure overloading was caused by a water hammer, which was created by the presence of sub-cooled water in the recirculation line when the pump was shut down. Subsequent draining of the line allowed steam to enter the space above the sub-cooled water, thereby creating the conditions conducive to water hammer due to bubble collapse. The FAC program in place at the time of rupture was believed to be fundamentally sound. Interaction with the operating or maintenance personnel was identified as the only way that the plant FAC engineer can know that a normally closed valve was not always fully seated or had been used to throttle flow.

Pleasant Prairie Unit 1 Feedwater Line Failure

On February 12, 1995, an instantaneous double-ended pipe break of a pipe tee occurred at the Pleasant Prairie Power Plant, which is a 630 MWe fossil power plant which began commercial operation in 1980 [19]. Two workers died as a result of the rupture. The broken feedwater line was made of seamless SA 106 C carbon steel. The pipe wall was thinned down to 0.090 inch (0.23 cm) thickness and failed under the normal operating pressure of 2000 psi (13.9 Mpa) at 450°F (232°C). The calculated one phase flow velocity was 40 ft/sec

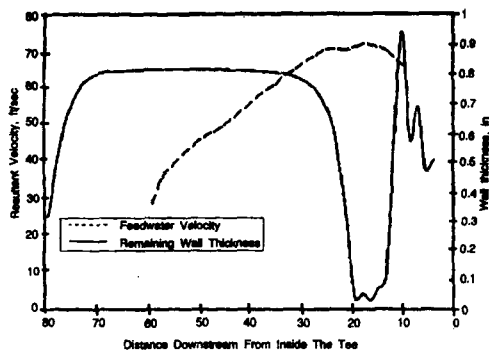


Fig. 14. Flow Assisted Corrosion: Correlation Between the Flow Velocity at the Branch Pipe Wall and the Remaining Wall Thickness Near the Circumferential Location of the Site of the Fail. Initiation[19]

(12.1 m/sec). The high level of FAC was due to high flow velocity, geometry, extremely low level of trace alloys (Cr), and feedwater chemistry. Flow path geometry may have caused turbulent flow against the pipe wall. The chromium content of the failed pipe was 0.01% while an upstream section had 0.12% which remained intact. Regarding feedwater chemistry, the average pH was 8.75 and oxygen content below 5 ppb. These conditions were enough to cause FAC. Fluid temperature of 450°F (232°C) was slightly above the peak FAC temperature of 355°F (180°C). Other conditions may have accelerated the thinning action. Figure 14 shows the relationship between feedwater velocity and pipe thinning.

5. Mitigation

Causes and effects of plant conditions on FAC have been well studied over the last twenty years as part of research and program developments. Those relatively well known factors can be summarized and some of areas, which are more

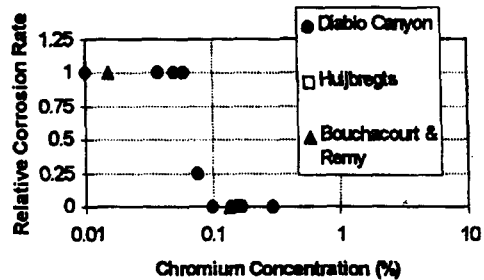


Fig. 15. Plant Experience Data for Effect of Chromium on FAC [3]

complicated and yet to be developed, can be identified.

Inspections

As mentioned in above, there are a number of systems and components of the secondary system which are most susceptible to FAC. These are based on industrial experiences and on model calculation activities. All carbon steel piping with less than one percent chromium with diameter 2 inches and larger are candidates for inspection [20]. Selection of areas for inspection is based on analytical evaluations which consider factors such as material composition, water chemistry, operating temperature, flow rate and geometry. Specific locations for examinations can be deduced from a system of ranking, with consideration of predicted wear rate and time to reach the required wall thickness. Usually pipe wall thickness is measured using ultrasonic techniques. A grid layout must be established to assure uniform examination of potentially affected zones. It is important that the readings be repeatable from inspection to inspection. A method of on-line inspection is being developed at MIT under support of Korea Electric Power Corporation using the direct current potential

drop method to avoid the cumbersome work of removing piping insulation as in case of ultrasonic testing. Direct current input points can be established nearby the susceptible areas.

Material Selection

According to a recent paper [3], a chromium content of 0.1% will result in resistance to flow accelerated corrosion. This effect is illustrated in Figure 15. The commonly used material A106 Grade B specification calls for less than 0.4% chromium, 0.4% copper and 0.15% molybdenum (ASTM 1988). The chromium content can vary from component to component within a piping system due to minor variations in the manufacturing process. Within the acceptable range of the minor elements in the specification, the rate of FAC can vary by as much as an order of magnitude. A portable alloy analyzer can be used to analyze all the components concerned [21]. A chemical analysis sampling program may show that a large proportion of the system components contain chemical compositions that will significantly influence their FAC rates. The eventual solution to the FAC problem may be replacement with higher alloys of at least 0.1% Cr content or above within the specified range.

Water Chemistry

In order to limit the rate of FAC in carbon steels a sufficiently high pH must be maintained. With morpholine treatment, the recommended range of a room temperature pH is 9.2 - 9.7. The upper limit is a compromise between operating at high pH to minimize the corrosion of steel, and minimizing the cost of operating the blowdown demineralizer. Beaver Valley Power Station used a combination

morpholine/hydrazine treatment and showed a factor of approximately three reduction in iron levels in the feedwater over treatment without morpholine [22]. EPRI PWR Secondary Chemistry Guidelines(Revision 2) issued in 1988 recommends morpholine to reduce FAC of secondary system components. When the pH at the temperature was calculated, it was found that the effective pH(t) of morpholine increased compared to the pH(t) of the equivalent ammonia solution as temperature(t) increased. For Beaver Unit 1, no piping components have been shown to exhibit significant FAC wear.

Oxygen Level

FAC in carbon steels in pure water decreases up to two order of magnitude when the oxygen concentration increases from 1 to 200 ppb. Only a very low quantity of oxygen is sufficient to convert ferrous to ferric ions in pure, alkaline water. In the presence of oxygen hematite precipitates and grows at the oxide/water interface or within the pores. Moreover, oxygen can promote the transformation of magnetite normally present at the oxide/water interface to hematite. The solubility of hematite is several orders of magnitude less than that of magnetite. Thereby, the FAC rate is reduced. In practice, additions of at least 30 ppb to the feedwater can be the basis of the oxygen-dosed neutral water chemistry and oxygen-ammonia treatment used for fossil plants [3].

Temperature

Liquid temperature is known to influence the chemical reaction during the FAC process as well as the protective layer formation. Moreover, the parameters characterizing the liquid layer close to the pipe wall like density,

viscosity etc are influenced by the temperature. The overall temperature effect on material loss due to FAC can be described by a bell-shaped curve which reaches a maximum at around 355°F (180°C) for wet steam conditions. The maximum is the result of competition between two reactions. The first is the formation rate of $\text{Fe}(\text{OH})_2$ which increases with temperature below the maximum. The other is formation of a protective layer of magnetite, which becomes less porous with the formation of hematite at higher temperatures. Also, the maximum solubility of magnetite occurs at 285-300°F (140-150°C) [23]. In single phase flow most FAC occurs within the temperature range 175-450°F (80-230°C). For two phase flow the range is somewhat higher, 285-500°F (140-260°C). However, considerable differences may exist in the values of the maximum temperature.

Hydrodynamic Factors

The most influential factor is mass transfer which carries away the dissolving ferrous ions from the corroding wall. As mentioned earlier various models have been proposed for both single and two phase flows. The flow state may be dictated by the thermodynamic state of fluid and steam. Moreover, the flow may become turbulent with changes in pipe geometry. In some cases it develops into impinging liquid drops against the pipe wall with severe erosion loss. There are almost always components (such as valves and orifices) and subsystems (such as feedwater pump recirculation lines) [24], where flow velocities can become very high locally, where the dynamic pressure may also result in evolution of bubbles of dissolved gasses or steam bubbles and cavities. When subcooled water is combined with trapped steam, even water hammer events can occur [25]. Thus, overall

mechanistic and empirical models can predict amount of FAC within reasonable range although peculiar areas may become very susceptible due to particular flow conditions.

6. Conclusions

In this paper we have reviewed the character of the FAC process. Additionally, several examples of FAC have been briefly discussed. Lastly, mitigation methods have been outlined. While the elimination of FAC can be achieved by replacement of piping with material with higher chromium content there remains a very large fraction of existing piping that is at risk for FAC. For this piping the control of water chemistry should be coupled with a well thought out program of monitoring and inspection.

References

1. Chexal, B. *Presentation at MIT Nuclear Engineering Department Seminar Series*. Cambridge, Sept. 16, (1996).
2. Kastner, W. et. al., *VGB Kraftwerkstechnik* **70**, 11, pp. 806-815, (1990).
3. Chexal, B. et. al., *Flow Accelerated Corrosion in Power Plants*, Pleasant Hill, CA: EPRI, (1996).
4. Kastner, W. and Nedelko, L., *Symposium: Plant Life Extension (PLEX) of Nuclear Power Plants*, April 24-26, (1991).
5. Keck, R. G., MIT PhD Thesis, (1987).
6. Sanchez-Caldera, L.E., *MIT PhD Thesis*, (1984).
7. Keller, V.H., *Kraftwerkstechnik*, **54**, p. 292, (1974).
8. Heitmann, H.G., and Kastner, W., *VGB Kraftwerkstechnik* **64**, 5, p. 1023-1029, (1984).
9. Kastner, W., *EPRI Workshop on Erosion-*

- Corrosion of Carbon Steel Piping-Nuclear and Fossil Plants*, April 14-15, (1987).
10. Bignold, G.J. et. al., *Proceedings of the Third Meeting on Water Chemistry of Nuclear Reactors*, British Nuclear Engineering Society, p. 219-226 (1983).
 11. Sweeton, F. H., and Baes, C. F., *Journal of Chemical Thermodynamics*, **2**, p.49, (1970).
 12. Bush, S.H. et. al. *Piping Failures in United States Nuclear Power Plants: 1961-1995*
 13. SKI Reprt 96:20, *Swedish Nuclear Power Inspectorate SKI Reprt 96:20*, Jan, (1996).
 14. Jonas, O., *NUREG/CR-5149*, Mar., (1988).
 15. Zysk, G.W. et. al., *Pressure Vessels and Piping Codes and Standards*, **338**, ASME, (1996).
 16. McNarr, T., *NRC LER Report*, May 1, (1991).
 17. Kupinski, M. et. al., *Pressure Vessels and Piping Codes and Standards*, **259**, ASME, (1993).
 18. Kupinski, M. et. al., *Pressure Vessels and Piping Codes and Standards*, **338**, ASME (1996).
 19. Patulski, S.A., *Joint Power Conference PWR*, **28**, ASME (1995).
 20. Deardorff, A. et. al., *Pressure Vessels and Piping Codes and Standards*, **238**, ASME (1992).
 21. Goyette, L.F. and Zysk, G.W., *Pressure Vessels and Piping Codes and Standards*, **259**, ASME, (1993).
 22. Finke, J.F. and Linnenbom, V.J., Jr., *Pressure Vessels and Piping Codes and Standards*, 259, ASME (1993).
 23. Kastner, W. et. al., *VGB Kraftwerktechnik*, 64, 5, p 411-423, May, (1984).
 24. Chandra, S. et. al., *Pressure Vessels and Piping Codes and Standards*, **285**, ASME (1994).
 25. Esselman, T.C. and Kupinski, M., *Pressure Vessels and Piping Codes and Standards*, **338**, ASME (1996).